Experimental study and analytical modeling of the channel length influence on the electrical characteristics of small-molecule thin-film transistors

W.Boukhili [a, b,*], M. Mahdouani[a], R. Bourguiga[a], J. Puigdollers[b]

[a]Laboratoirede Physique des Matériaux : Structure et Propriétés, Groupe Physique des Composants et Dispositifs Nanométriques, Faculté des Sciencesde Bizerte, 7021 Jarzouna-Bizerte, Université de Carthage, Tunisia.

[b]Department d'Enginyeria Electronica, Universitat Politecnica de Catalunya, C/Jordi Girona, Modul C4, 08034 Barcelona, Spain.

ABSTRACT

Bottom-contact p-type small-molecule copper phthalocyanine (CuPc) thin film transistors (TFTs) with different channel lengths have been fabricated by thermal evaporation. The influence of the channel length on the current-voltage characteristics of the fabricated transistors were investigated in the linear and saturation regimes. The devices exhibit excellent p-type operation characteristics. Results show that devices with smaller channel length (L=2.5µm and 5µm) present the best electrical performance, in terms of drain current value, field effect mobility and subthreshold slope. Saturation field-effect mobilities of $1.7x10^{-3}$ $cm^2V^{-1}s^{-1}$ and $1x10^{-3}cm^2V^{-1}s^{-1}$ were obtained for TFTs with channel lengths of L = 2.5µm and L= 5µm, respectively. Transmission line method was used to study the dependence of the contact resistance with the channel length. Contact resistance becomes dominant with respect to the channel resistance only in the case of short channel devices (L=2.5µm and 5µm). It was also found that the field effect mobility is extremely dependent on the channel length dimension. Finally, an analytical model has been developed to reproduce the dependence of the transfer characteristics with the channel length and the obtained data are in good agreement with the experimental results for all fabricated devices.

Keywords: p-type small-molecule; Channel length effect; Contact and channel resistances; Variable range hopping (VRH) model.

* Corresponding author: wboukehili@yahoo.fr (Walid Boukhili)

1. Introduction

Over the recent years, electronic devices based on organic semiconductors, such as organic light-emitting diodes (OLEDs), organic photovoltaic cells and organic thin film transistors (OTFTs) have been the subject of intense research. Among them, OTFTs have gained a high interest and have made a tremendous progress from the viewpoint of electronic performance and reliability. The simple processing procedures, using low temperature deposition and solution processing methods, hold promise for cheaper, lightweight, mechanical flexibility and low-cost fabrication [1-3], making organic devices a basic component of a wide range of viable technology. Promising applications of OTFT include gas and image sensors, smart cards, active-matrix displays, radio-frequency identification tags and flexible microelectronics [4-8]. Among the wide variety of organic semiconductors considered, metal phthalocyanine (metal-Pc) has been widely studied as a standard organic semiconductor to be used in the fabrication of organic electronic devices [9-12]. Copper phthalocyanine (CuPc) is a p-type organic semiconductor material, which have been mass-produced in relatively high yields for many years and known to be one of the most robust organic compounds with excellent thermal and chemical stability in ambient conditions [13]. Several studies have been focused and performed for characterizing and improving the performances of CuPc based TFTs[9-14].Indeed, a high mobility up to 0.02 $cm^2V^{-1}s^{-1}$ and on/off ratio around of 10^5 for CuPc-TFTs have been reported [10]. Puigdollers et al. reported that the field effect mobility was around 0.2×10^{-4} for the CuPc-TFT using polymethylmethacrylate (PMMA) as a polymer gate dielectric [9]. F. Yakuphanoglu et al. [14] reported that CuPc-TFT was fabricated using p-SiO_2 as gate dielectric. They found that the CuPc activate layer indicates the homogeneous small crystal grains with a roughness of 3.878nm.

In this work, we report a systematic study of the channel length effects on the electrical performance of the CuPc-TFTs in the linear and saturation regimes. Accordingly, from the experimental curves the electrical parameters that characterize the CuPc-TFTs were extracted and correlated with the channel length variation. The influence of the channel length and contact resistance on the field effect mobility was also examined. Finally, we have developed an analytical model in order to reproduce the experimental transfer characteristics of the fabricated CuPc-TFTs for several channel lengths.

2. Experimental details

The chemical structure of the copper phthalocyanine (CuPc) is given in fig. 1 (a). CuPc was commercially available from Aldrich chemical (98% purity) and no further purification process was performed. A schematic device cross section of the studied CuPc-TFT is shown

in fig. 1(b). All CuPc-TFTs were constructed on heavily doped n-type silicon wafers (n-Si) as a common bottom-gate electrode with 200nm thick thermally grown silicon dioxide (SiO_2) as a gate dielectric layer. For the source and drain (S-D) electrodes, Au (30nm)/ITO (3nm) double layer was used and patterned by conventional lift-off technique. The bottom ITO layer (3nm thick) is employed to promote the adhesion of the Au layer to the underlying SiO_2 surface. These substrates were purchased from the Fraunhofer IPMS Company. For the active layer, CuPc thin films were thermally evaporated using shadow mask in a high-vacuum system with a base pressure of $5x10^{-6}$ mbar. CuPc was deposited at room temperature with moderate deposition rates ($<5Å s^{-1}$). CuPc thickness was 50nm, as determined by means of a surface profilometer. In order to study the effects of the geometric dimensions on the electrical performance of the transistors, different CuPc-TFTs were fabricated on the same deposition process with different channel length (L). The studied channel lengths were 2.5µm, 5µm, 10µm and 20µm with a fixed channel width (W) of 2000µm. The electrical characterization of the fabricated devices was performed at room temperature and with moderate vacuum conditions (10^{-1} mbar) using a parameter analyzer (model HP5156).

3. Results and discussion

A typical scanning electronic microscopy planar view of 50 nm CuPc film deposited on SiO_2 is given in fig. 1(c). From this figure, it can be seen that the film was composed of homogeneous small crystal grains with an average diameter of 40–50 nm. These values were in good agreement with the crystallite sizes calculated from the XRD measurements [9].

3.1. Influence of the channel length on the output characteristics

The experimental output characteristics (drain current (I_D) versus drain voltage (V_D) curves for different gate voltages (V_G)) of the fabricated CuPc-TFTs with different channel lengths (L=2.5µm, 5µm, 10µm and 20µm) are depicted in figs. 2 (a)–(d). The output characteristics were obtained by scanning V_D from 0 to -80Vwith-0.8V increments for different gate voltages (V_G), ranging from 0 to -60Vwith a step of -10V. When V_D equals V_G-V_{th}, the electric field at the drain electrode is reduced to zero, the channel is pinched off, and drain current becomes independent of V_D (saturation region). In addition, the drain current increases with negative gate and drain voltages. For each channel length, we observe that the I_D–V_D curves clearly resemble those of p-type organic field effect transistor, suggesting that CuPc-TFT is a clear p-type semiconductor transistor that operates in accumulation mode. In order to better show the effect of the channel length on the output characteristics, in fig 2(e) we plotted the variation of

the drain current as function drain voltage at a fixed gate voltage of -60V. Fig. 2(e) shows that the output drain current increases about 15% when the channel length decreases from 20µm to 2.5µm.

For short channel lengths (L = 2.5µm and L= 5µm) the proximity of the drain and source electrodes can affect the conduction channel. This can enlarge the surface potential, making the channel more attractive to charge carriers (holes in our case), and decreasing the resistance of the channel. This could explain the higher conductivity observed in the transistor with a short channel [15].

3.2. Contact and channel resistances in CuPc-TFTs

It is well known that the interface properties between the source-drain (S-D) electrodes and the organic semiconductor layer play an essential role in the final OTFTs performance. The contact resistance provides a measure of the injection efficiency of carrier charges into the active layer of the OTFTs and characterizes the S-D electrodes/organic semiconductor interface. Several methods have been proposed to extract the contact resistance in OTFTs [16-20]. In our case the estimation of the contact resistance values was done using the transfer line method (TLM) [17-18].

Therefore, in the frame of the TLM method, the measured total resistance (R_{Tot}) of the device can be modeled as the sum of two series resistances as follows [17-18]:

$$R_{Tot} = R_C + R_{ch}(L) = R_C + \frac{L}{WC_i \mu_{FET,lin} (V_G - V_{th})} \quad (1)$$

where $R_C = R_S + R_D$ is the resistance associated to the drain and source contacts, R_{ch} is the channel resistance, which linearly depends on the channel length. R_{Tot} is the experimental total resistance, which was determined from the linear regime of the output characteristics in the linear regime ($R_{Tot} = [\frac{\partial V_D}{\partial I_D}]_{V_D \to 0}^{V_G}$) for different high negative gate voltages (V_G = -20V, -30V, -40V,-50V and -60V) and for several channel lengths (fig. 3(a)).

Fig. 3(a) shows that R_{Tot} increases linearly with increasing channel length (L). The intersection with the Y-axis of the R_{Tot} versus L curve, when the channel length becomes zero, provides an estimation of the R_c value. The obtained values of $R_c$as a function of the channel length are depicted in fig. 3(b).We can observe that the R_c values decreases with increasing the gate voltage. This dependence can be explained by the additional increase of the carrier density in the accumulation channel near the contacts (S-D). The same behavior is observed for the dependence of R_{ch} with the channel length. As seen in fig. 3(b),R_{ch} is higher than R_c

only for the channel lengths equal to 2.5µm and 5µm. From fig.3 (b), we found that when the channel length is reduced, the channel resistance decreases. Indeed, when L decreases, R_c becomes not negligible compared to R_{ch} and tends to reduce the transconductance and the mobility of the CuPc-TFTs at high negative gate voltages. We conclude that for channel lengths less than L =5µm the electrical performance of the CuPc-TFTs are mainly limited by the contact resistance rather than by the channel resistance.

3.3. Transfer characteristics and electrical parameters extraction

Generally speaking, the electrical transfer characteristics (dependence of the drain current (I_D) versus the gate voltage (V_G) at fixed drain voltage (V_D)) provide a better method to examine electrical performances of such OTFT in the linear and in the saturation regime.

The transfer characteristics of OTFTs can be analyzed in the linear regime (under low drain voltage) by the following equation [21-22]:

$$I_D = \frac{W}{L} C_i \mu_{lin} \left(V_G - V_{th} - \frac{V_D}{2} \right) V_D \quad (2)$$

where W and L is the channel width and length, C_i is the capacitance of the insulator per unit area, V_{th} is the threshold voltage and μ_{lin} is the linear mobility.

Fig. 4(a) shows the transfer characteristics in the linear regime of the CuPc-TFTs measured from 0 to -60Vwith-10V increments with a fixed drain voltage (V_D) of -5V. As seen in fig. 4(a) that at low drain voltage (V_D= -5V) the drain current increases as the channel length was decreased from 20µm to 2.5µm.

Based on this experimental data, the intrinsic electrical parameters such as transconductance and linear mobility have been extracted for each channel length in the linear regime. The transconductance (g_m) is a measure of device gain and is directly related to the device switching speed and is defined as [23-25]:

$$g_m = \left[\frac{\delta I_D}{\delta V_G} \right]_{V_{D=cte}} = \frac{W}{L} \mu_{lin} C_i V_D \quad (3)$$

In addition to g_m, another important parameter is the field-effect mobility, which is generally gate voltage dependent, and can be determined in the linear regime (V_D= -5V) by using the expression of g_m[23-25]:

$$\mu_{lin} = \frac{L}{C_i V_D W} \left[\frac{\delta I_D}{\delta V_G} \right]_{V_{D=cte}} = \frac{L}{C_i V_D W} g_m \quad (4)$$

The experimental values of g_m and μ_{lin} in linear regime as function of V_G for CuPc-TFTs with different channel lengths are depicted in fig. 4(b) and (c), respectively.

We found that g_m and μ_{lin} increase linearly with the gate voltage for low V_G and decrease for high V_G in all the studied devices. This behavior is more pronounced for devices with smaller channel lengths. The decreasing of the g_m and μ_{lin} values for high V_G voltages could be explained by the decrease of the drain current. The decrease of the drain current is due to the high electrical resistance between S-D electrodes and the organic semiconductor [26].

At high V_D, the OTFTs operate in the saturation regime, and the I_D tends to saturate as the conducting channel is pinched off. The drain current expression becomes [21-22]:

$$I_D = \frac{W}{2L} C_i \mu_{sat} (V_G - V_{th})^2 \quad (5)$$

where μ_{sat} is the field effect mobility in the saturation regime.

Fig. 5(a) shows the transfer characteristic curves (I_D versus V_G) in saturation regime of the fabricated transistors, in which V_G is swept from 0 to -60 V (with -10V increments) and with a fixed V_D=-70V.Fig.5(a) shows that the obtained saturation I_D for the short channel transistor (L= 2.5µm) is about 10% higher that the I_D obtained for the long channel transistor (L=20µm).Several papers have reported that the field-effect mobility in thin-film semiconductors is limited by the grain boundaries of the polycrystalline film [27]. Since CuPc films are composed of nanocrystalline grains, we can speculate that the observed decrease of the drain current for long channel length devices is due to the higher presence of grain boundaries in the active layer of the transistor. These grain boundaries act as trap centers for free charge carriers. By plotting the square root of the drain current versus gate voltage curve ($|I_{D,sat}|^{1/2}$ versus V_G) in the saturation regime (V_D= -70V) we can evaluate the threshold voltage (V_{th}) values. V_{th} is extracted from the intersection of the linear part of the square root of I_D with the V_G axis in the saturation regime (in fig. 5(b) is shown for the transistor with L=2.5µm). The dependence of V_{th} with channel length is reported in table 1. This table shows that when channel length is reduced from 20 to 2.5µm, the threshold voltage shifts to positive values. It is assumed that the shift of the threshold voltage in organic TFTs is directly related to the total trapped charge density at the insulator/organic semiconductor interface [28-29], and can be determined by:

$$N_{trap} = \left|\frac{V_{th} C_i}{q}\right| \quad (6)$$

In the saturation regime (V_D= -70V), the experimental saturation mobility is calculated by using the following formula:

$$\mu_{sat} = \frac{2L}{WC_i}\left(\frac{\partial\sqrt{|ID|}}{\partial V_G}\right)^2 \quad (7)$$

The dependence of the saturation mobility with gate voltage (V_G) and channel length (L) is shown in fig. 5(c). It is observed that μ_{sat} increases linearly with gate voltages for low negative V_G and decreases at high negatives V_G for each value of L. This decrease of the saturation field effect mobility is mainly attributed to the existence of contact resistance (R_c) between S-D electrodes/organic semiconductor interface. From fig. 5(c) we have extracted the maximum values of saturation mobility, which are plotted as function the channel resistance in fig. 5(d).

Figure 6 shows the variation of the drain current in logarithmic scale versus V_G for each channel length at V_D= -70V, which is used to extract the turn-on voltage (V_{on}) and the current ratio (I_{on}/ I_{off}). I_{on}/ I_{off} is defined as the ratio of the maximum drain current at a certain gate voltage to the drain current at zero gate voltage, and reflects the commutation properties of the device to the current variation. The subthreshold slope (SS) is defined as the voltage required for increasing the drain current by a factor of 10. From the transfer characteristics we can determine SS through the following relation [16, 23]:

$$SS = \left[\frac{dlog(I_D)}{dV_G}\right]^{-1} \quad (8)$$

and from the SS values we can infer the density of the interface trap in the CuPc-TFTs by using the following expression [16, 23]:

$$D_{it} = \left[\frac{SSlog(e)}{kT/q} - 1\right]\frac{C_i}{q} \quad (9)$$

where T is the temperature, k is Boltzmann's constant and q is the electronic charge.

The extracted electrical parameters of the CuPc-TFTs with several channel lengths are summarized in table 1.

4. Modeling of the transfer characteristics via variable range hopping (VRH) model: Application to CuPc-TFTs

So far the conventional crystalline semiconductor MOSFET theory presented and used as a reference for describing the behavior of OTFTs operation. For a good understanding of the transport properties of charge carriers in OTFTs, many of models have been introduced and developed. Furthermore, the modeling of OTFTs has left its infancy and has reached a level whereby a good agreement is reached with the experimental characteristics [26, 27, 30-32].

In the disordered amorphous structure of organic materials, the charge transport is occurred by variable range hopping (VRH) of charge carriers between strongly localized states [33-37]. The VRH model was proposed by Vissenberg and Matters in order to model the electrical

characteristics OTFTs [33]. It considers the hopping percolation of charge carriers between the localized states.

In order to obtain an analytical expression of the drain current based on the variable range hopping model, it is assumed that the current transport is parallel to the insulator–semiconductor interface [38]. Indeed, in combination with percolation [39-41] and variable range hopping theory, the conductivity expression is defined as follows [33]:

$$\sigma(\delta,T) = \sigma_0 \left[\frac{\pi N_t \delta \left(\frac{T_c}{T}\right)^3}{(2\alpha)^3 B_c \Gamma\left(1-\frac{T}{T_c}\right)\Gamma\left(1+\frac{T}{T_c}\right)} \right]^{\frac{T_c}{T}} \tag{10}$$

where σ_0 is the percolation prefactor of the conductivity, which it has a meaning of a material specific conductivity, α is an effective overlap parameter that governs the tunneling process between two localized states, B_c is the critical number of bonds per site in the percolating network, for a three-dimensional amorphous system, $B_c \cong 2$ [40-41].$\Gamma(x) = \int_0^{+\infty} dy exp^{(-y)} y^{(x-1)}$ is the gamma function, T_c is the characteristic temperature. N_t is the number of states per unit volume and δ is the fraction of the localized states occupied by a carrier.

According to the developed theory in [33], the sheet conductance can be expressed as follows [38]:

$$g_{sh} = \sigma_0 \sqrt{\frac{2\varepsilon_0 \varepsilon_s K_B T_c}{\delta_0 N_t}} \frac{K_B T}{q(T-2T_c)} \frac{W}{L} \left[\left(\frac{V_G - V_{th}}{\frac{(2\alpha)^3 B_c 2\varepsilon_0 \varepsilon_s K_B T_c}{C_i^2 \left(\frac{T_0}{T}\right)^3 sin\left(\pi \frac{T_c}{T}\right)}} \right)^{\frac{2T_c}{T}-1} - 1 \right] \tag{12}$$

For the purpose of refining this last expression, we assume that:

$$\beta = \sigma_0 \sqrt{\frac{2\varepsilon_0 \varepsilon_s K_B T_c}{\delta_0 N_t}} \frac{K_B T}{q(T-2T_c)} \text{ and } \rho = \frac{(2\alpha)^3 B_c 2\varepsilon_0 \varepsilon_s K_B T_c}{C_i^2 \left(\frac{T_c}{T}\right)^3 sin\left(\pi \frac{T_c}{T}\right)}$$

Therefore, the final expression of the sheet conductance given by:

$$g_{sh} = \beta \frac{W}{L} \left[\left(\frac{V_G - V_{th}}{\rho} \right)^{\frac{2T_c}{T}-1} - 1 \right] \tag{13}$$

Using this expression for the simplified sheet conductance, the drain current I_D can be calculated by [42–43]:

$$I_D = \frac{W}{L} \int_{V_G - V_{th} - V_D}^{V_G - V_{th}} g_{sh}(V) dV \tag{14}$$

From Eqs. (13) and (14) the following expressions for the drain current are determined [33, 38, 43]:

$$I_D = \beta \frac{W}{L}\left[\left(\frac{V_G - V_{th}}{\rho}\right)^{\frac{2T_C}{T}} - \left(\frac{V_G - V_{th} - V_D}{\rho}\right)^{\frac{2T_C}{T}}\right] \quad (15)$$

in the linear regime if$|V_G - V_{th}| > |V_D|$

$$I_D = \beta \frac{W}{L}\left(\frac{V_G - V_{th}}{\rho}\right)^{\frac{2T_C}{T}} \quad (16)$$

in the saturation regime if $|V_G - V_{th}| < |V_D|$

By using Eqs. (25) and (26), the transfer characteristic curves in the linear and saturation regimes were reproduced for each device. The fitting parameters σ_0 ,$2T_c/T$ and $\alpha^{-1}$are given in table 2. A good agreement between the experimental transfer characteristics data and the model described here has been obtained for each channel length (fig.7 (a)-(d)). Comparing the measured transfer characteristics and those modeled, we conclude that the model correctly describes the electrical characteristics of CuPc-TFTs.

5. Conclusions

CuPc based organic thin film transistors with different channel lengths were successfully fabricated and characterized. We have examined the effects of the channel length variation on the electrical characteristics of the devices (output and transfer characteristics) and on the key electrical parameters such as transconductance, linear and saturation mobility the threshold voltage of the CuPc-TFTs. It's found that the CuPc-TFTs with relatively short channel (L=2.5µm and L=5µm) exhibited a better performance in terms of the drain current, transconductance and mobility, but reveal a strong influence of the contact resistance on electrical parameters in terms of mobility and conductance. The reduction of the channel lengths may improve of the CuPc-TFTs performance. By using the TLM, the total channel and contact resistances were extracted for all fabricated devices. We conclude that for channel lengths less than L = 5µm the electrical performance of the CuPc-TFTs are mainly limited by the contact resistance rather than by the channel resistance. Besides, a VRH charge transport model able to reproduce accurately the experimental transfer characteristics has been successfully applied for the CuPc-TFTs. The modeled results show an excellent agreement with the experimental data in term of transfer characteristics in the linear and saturation regime.

Acknowledgements

This work has been supported by the Spanish ministry of science under project TEC2011-27859-C02-01 and the Tunisian Ministry of Higher Education and Scientific Research, University of Carthage.

References

[1] C.L. Fan, Y.Z. Lin, W.D. Lee, S.J. Wang, C.H. Huang, Org. Electron. 13 (2012) 2924.

[2] C.Y. Wei, F. Adriyanto, Y.J. Lin, Y.C. Li, T.J. Huang, D.W. Chou, Y.H. Wang, IEEE Electron Dev. Lett. 30 (2009) 1039.

[3] C.L. Fan, P.C. Chiu, C.C. Lin, IEEE Electron Dev. Lett. 31 (2010) 1485.

[4] K.S. Narayan, N. Kumar, Appl. Phys. Lett. 79 (2001) 1891-1893.

[5] K.S. Narayan, A.G. Manoj, Th.B. Singh, A.A. Alagiriswamy, Thin Solid Films 417(2002) 75-77.

[6] H.E. Katz, Chem. Mater. 16 (2004) 4748.

[7] H. Nakanotani, S. Akiyama, D. Ohnishi, M. Moriwake, M. Yahiro, T. Yoshihara, S. Tobita, C. Adachi, Adv. Funct. Mater. 17 (2007) 2328.

[8] M. Berggren, D. Nilsson, N.D. Robinson, Nat. Mater. 6 (2007) 3.

[9] J. Puigdollers, C. Voz, M. Fonrodona, S. Cheylan, M. Stella, J. Andreu, M. Vetter, R. Alcubilla, J. Non-Cryst. Solids 352 (2006) 1778–1782.

[10] Z. Bao, A. J. Lovinger, A. Dodabalapur, Appl. Phys. Lett. 69 (1996) 3066.

[11] S. Hoshino, T. Kamata, K. Yase, J. Appl. Phys. 92 (2002) 6028.

[12] K. Xiao, Y. Liu, G. Yu, D. Zhu, Synth. Met.137 (2003) 991.

[13] N. Kobayashi, T. Furuyama, K. Satoh, J. Am. Chem. Soc. 133 (2011) 19642-19645.

[14] F. Yakuphanoglu, M. Caglar, Y. Caglar, S. Ilican, Synth. Met.160 (2010) 1520–1523.

[15] S. Chopra, R.S. Gupta, Microelectron. Eng. 54 (2000) 263–275.

[16] W. Boukhili, M. Mahdouani, M. Erouel, J. Puigdollers, R. Bourguiga, Synth. Met.199 (2015) 303–309.

[17] J. Kanicki, F.R. Griffith, J. Griffith, R. Ploastre, J. Appl. Phys. 69 (1991) 2339.

[18] D. Natali, M. Caironi, Adv. Mater. 24 (2012) 1357.

[19] R. Bourguiga. M. Mahdouani, S. Mansouri, G. Horowitz, Eur. Phys. J. Appl. Phys. 39 (2007) 7–16.

[20] Y. J. Lin, B. C. Huang, Microelectron. Eng. 103 (2013) 76-78.

[21] S. M. Sze, Physics of Semiconductor Devices, Wiley InterScience, New York, 1981.

[22] R.F. Pierret, Semiconductor Device Fundamentals, Addison-Wesley Publishing Company, 1996.

[23] G. Horowitz, Adv. Funct. Mater. 13 (2003) 53.

[24] G. Horowitz, R. Hajlaoui, D. Fichou, A. El Kassmi, J. Appl. Phys. 85 (1999) 6.

[25] R. Bourguiga, F. Garnier, G. Horowitz, R. Hajlaoui, P. Delannoy, M. Hajlaoui, H. Bouchriha, Eur. Phys. J. Appl. Phys. 14 (2001) 121.

[26] S. Mansouri, M. Mahdouani, A. Oudir, S. Zorai, S. Ben Dkhil, G. Horowitz, R. BourguigaEur. Phys. J. Appl. Phys. 48 (2009) 30401.

[27] F. Yakuphanoglu, W. A. Farooq, Synth. Met. 161 (2011) 132–135.

[28] A. Bolognesi, M. Berliocchi, M. Manenti, A.D. Carlo, P. Lugli, K. Lmimouni, C. Dufour, IEEE Trans. ElectronDev. 51 (2004) 1997.

[29] K.P. Pernstich, S. Haas, D. Oberhoff, C. Goldmann, D.J. Gundlach, B. Batlogg, A.N. Rashid, G. Schitter, J. Appl. Phys. 96 (2004) 6431.

[30] G. Horowitz, R. Hajlaoui, H. Bouchriha, R. Bourguiga, M. Hajlaoui, Adv. Mater. 10 (1998) 923–927.

[31] B. Kumar, B.K. Kaushik, Y.S.Negi, S.Saxena, G.D.Varma, MicroelectronicsJournal 44 (2013) 736–743.

[32] S. Zorai, R. Bourguiga, Eur. Phys. J. Appl. Phys. 59 (2012) 20201.

[33] M. C. J. M. Vissenberg, M. Matters, Phys. Rev. B 57 (1998) 12964.

[34] H. B*ä*ssler, Phys. Status Solidi B 175 (1993) 15.

[35] M. Schwoerer, H. C. Wolf, Organic Molecular Solids, Wiley-VCH, Weinheim, 2007.

[36] P. M. Borsenberger, R. Richert, H. B*ä*ssler, Phys. Rev. B 47 (1993) 4289.

[37] M. Estrada, I. Mejia, A. Cerdeira, J. Pallares, L. Marsal, B. Iniguez, Solid State Electron. 52 (2008)787.

[38] Ling Li, Hans Kosina, "An analytical model for organic thin film transistors", Conference on Electron Devices and Solid-State Circuits (EDSSC)Hong Kong, IEEE, (2005) 571-574.

[39] V. Ambegaokar, B. I. Halperin, J. S. Langer, Phys. Rev. B 4 (1971) 2612.

[40] M. Sahimi, Applications of Percolation Theory, Taylor & Francis, London, 1994.

[41] G. Pike, C. Seager, Phys. Rev. B 10 (1974) 1421-1434.

[42] G. Horowitz, P. Delannoy, J. Appl. Phys. 70 (1991) 469.

[43] E. Calvetti, L. Colalongo, Zs. M. Kovács-Vajna, Solid-State Electron. 49 (2005) 567.

Figures captions

Figures 1 (a)-(c): **(a)** A schematic view of the molecular structure of copper phthalocyanine. **(b)** Cross section of Bottom Gate Bottom Contact CuPc-TFTs with its bias condition.**(c)** A scanning electron microscopy image of 50 nm CuPc films deposited on SiO_2 at room temperature.

Figures 2 (a)–(e): (a) - (d): Output characteristics curves of CuPc-TFTs with different channel lengths (L =2.5µm, 5µm, 10µm and 20µm). **(e)** Output characteristics of the CuPc-TFTs at high negative gate voltage (V_G= -60V) with different channel lengths.

Figures 3 (a)-(b): **(a)** Total device resistance versus channel length of the CuPc-TFTs at different high negative gate voltages (V_G= -20, -30, -40, -50, -60V). **(b**) Contacts and channel versus gate voltage for each channel length.

Figures 4 (a)-(c): (a) Transfer characteristics (I_D versus V_G plots) measured in the linear regime for different channel lengths (L=2.5µm, 5µm, 10µm and 20µm). **(b)** Transconductance g_m as function V_G. **(c)** The experimental linear mobility versus V_G for all devices. **(c)** Maximum linear mobility versus channel resistance.

Figures 5 (a)-(c): (a) Transfer characteristics I_D versus V_G plots measured in the saturation regime at V_D = -70V for all CuPc-TFTs. **(b)**The square root of the drain current versus gate voltages curve in saturation regime for L=2.5µm. **(c)** Experimental saturation mobility versus V_G for each channel length. **(d)** Maximum saturation mobility versus channel resistance.

Figure 6: The variation of the drain current in logarithmic scale versus V_G at V_D= -70V: extraction method of the parameters: the turn-on voltage and the ratio current.

Figures 7(a) - (d): The good agreement between experimental (circle line) and that obtained from model (full line) transfer characteristics of CuPc-TFTs**:(a)** in linear regime for L=2.5µm and L=5µm. **(b)** in linear regime for L=10µm and L=20µm. **(c)** in saturation regime for L=2.5µm and L=5µm. **(d)** in saturation regime for L=10µm and L=20µm.

Tables captions

Table 1. Extracted key parameters of the CuPc-TFTs with different channel lengths.

Table 2. Parameter values that give a good agreement between the measured transfer characteristics and those obtained by the model.

Parameters \ L(μm)	L=2.5μm	L=5μm	L=10μm	L=20μm
V_{th}(V)	-15	-17	-18	-23
$N_{trap}(cm^{-2})$	1.4×10^{12}	1.84×10^{12}	1.95×10^{12}	2.47×10^{12}
SS(V/dec)	15	12	6.5	3.2
D_{it} (cm^{-2} eV^{-1})	2.8×10^{13}	2.25×10^{13}	1.2×10^{13}	6×10^{12}
I_{on}/I_{off}	2×10^{4}	1.5×10^{4}	3.5×10^{3}	10^{3}
V_{on}(V)	-1	-2.5	-2	-6.5

Table 1

Parameters \ L(μm)	L=2.5μm	L=5μm	L=10μm	L=20μm
$\sigma_0(Sm^{-1})$	6.7×10^{6}	6.7×10^{6}	6.7×10^{6}	6.7×10^{6}
α^{-1}(Å)	1.6	2	2	2.3
$2T_c/T$	2.6	2.6	2.6	2.6

Table 2

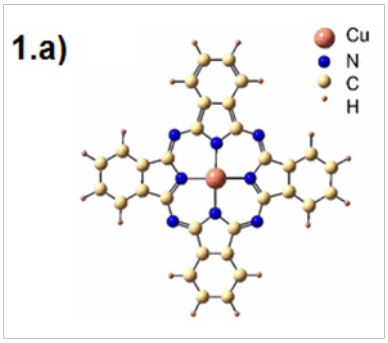

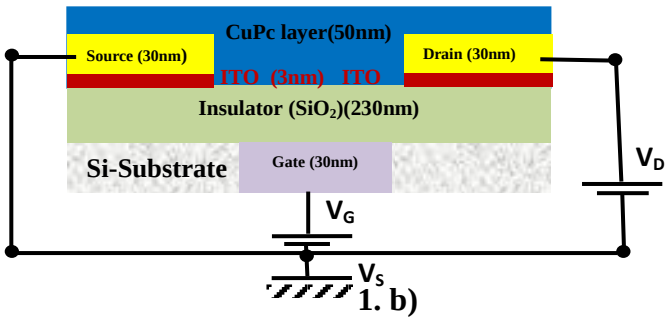

1. b)

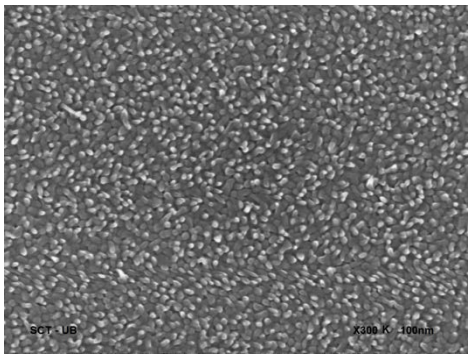

1.c)

Figures 1 (a)-(c)

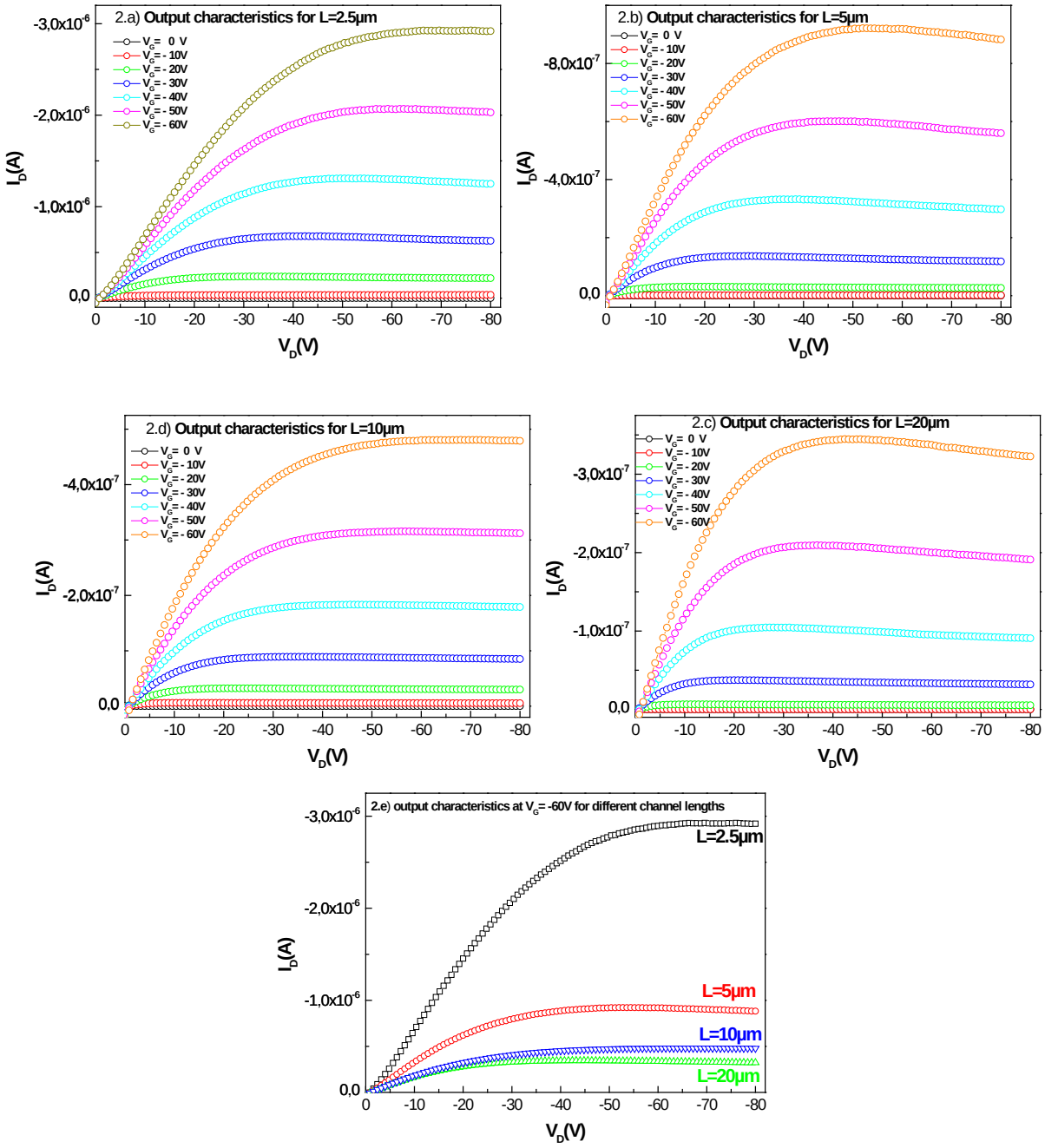
2.a) Output characteristics for L=2.5µm
2.b) Output characteristics for L=5µm
2.d) Output characteristics for L=10µm
2.c) Output characteristics for L=20µm
2.e) output characteristics at V_G= -60V for different channel lengths
L=2.5µm
L=5µm
L=10µm
L=20µm
I_D(A)
V_D(V)

Figures 2(a)-(e)

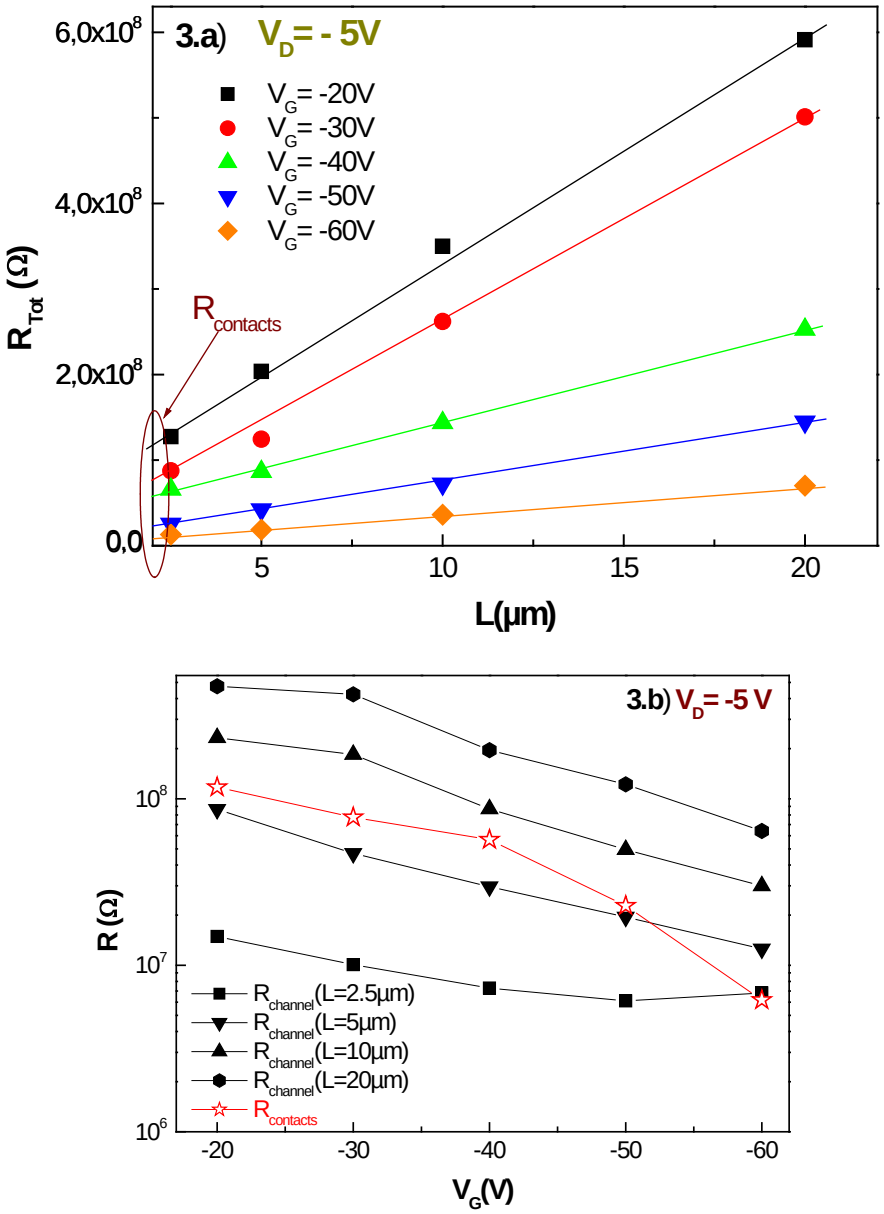
3.a) V_D= - 5V
V_G= -20V
V_G= -30V
V_G= -40V
V_G= -50V
V_G= -60V
$R_{contacts}$
R_{Tot} (Ω)
6,0x10^8
4,0x10^8
2,0x10^8
0,0
5
10
15
20
L(µm)
3.b) V_D= -5 V
R (Ω)
10^8
10^7
10^6
$R_{channel}$(L=2.5µm)
$R_{channel}$(L=5µm)
$R_{channel}$(L=10µm)
$R_{channel}$(L=20µm)
$R_{contacts}$
-20
-30
-40
-50
-60
V_G(V)

Figures 3(a)-(b)

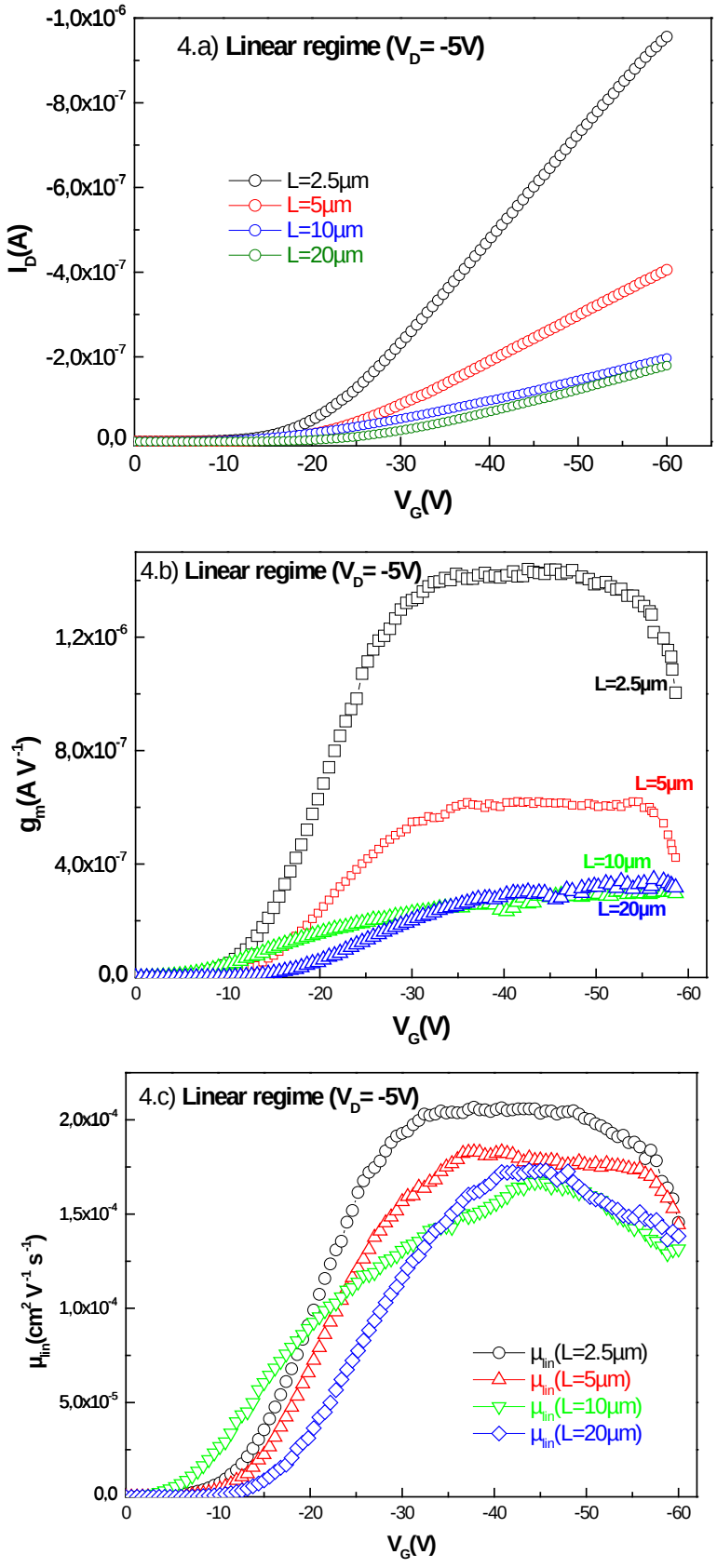
4.a) Linear regime (V_D= -5V)
L=2.5µm
L=5µm
L=10µm
L=20µm
I_D(A)
V_G(V)
4.b) Linear regime (V_D= -5V)
L=2.5µm
L=5µm
L=10µm
L=20µm
g_m(A V^-1)
V_G(V)
4.c) Linear regime (V_D= -5V)
µ_lin(L=2.5µm)
µ_lin(L=5µm)
µ_lin(L=10µm)
µ_lin(L=20µm)
µ_lin(cm^2 V^-1 s^-1)
V_G(V)

Figures 4(a)-(c)

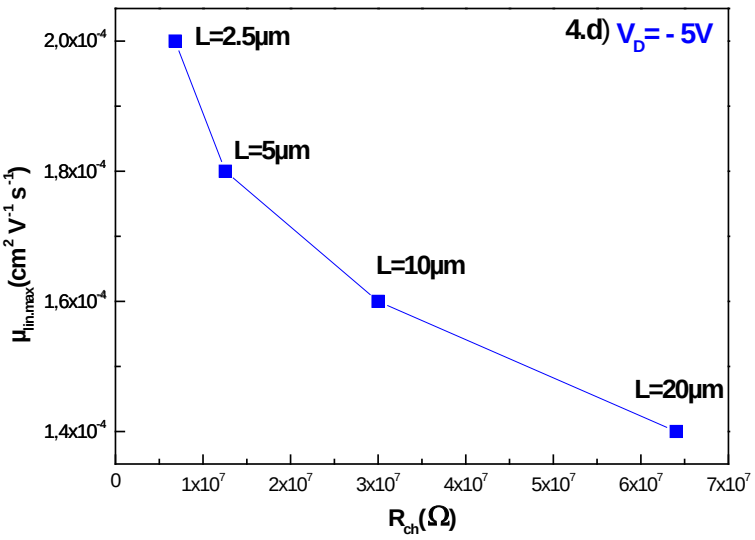
4.d) V_D= - 5V
L=2.5µm
L=5µm
L=10µm
L=20µm
2,0x10-4
1,8x10-4
1,6x10-4
1,4x10-4
$\mu_{lin,max}$(cm^2 V^{-1} s^{-1})
0
1x10^7
2x10^7
3x10^7
4x10^7
5x10^7
6x10^7
7x10^7
R_{ch}(Ω)

Figure 4 (d)

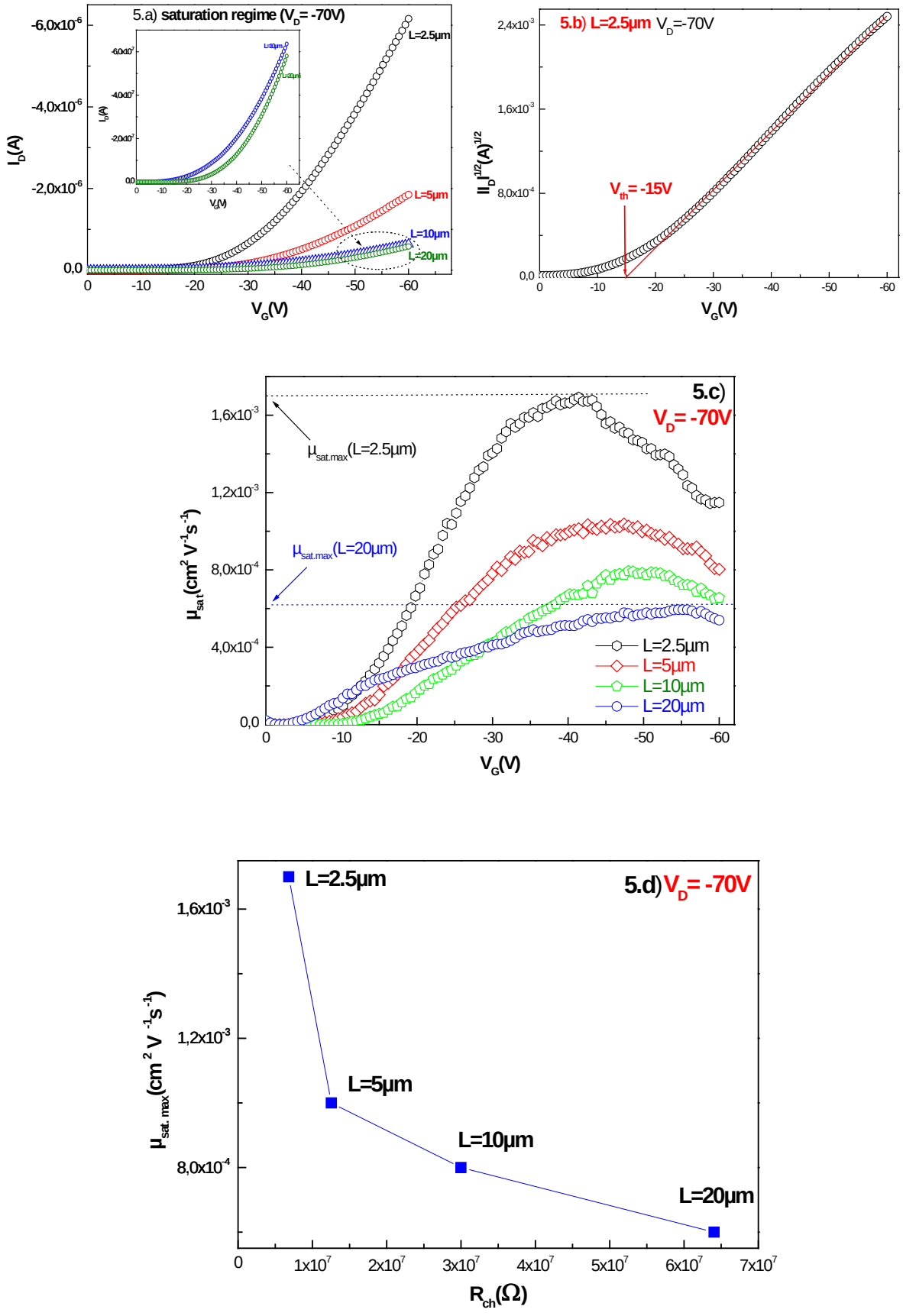
5.a) saturation regime (V_D= -70V)
L=2.5µm
L=5µm
L=10µm
L=20µm
I_D(A)
V_G(V)
5.b) L=2.5µm V_D=-70V
V_{th}= -15V
$I_D^{1/2}$(A)$^{1/2}$
V_G(V)
5.c)
V_D= -70V
$\mu_{sat.max}$(L=2.5µm)
$\mu_{sat.max}$(L=20µm)
μ_{sat}(cm^2 V^{-1}s^{-1})
L=2.5µm
L=5µm
L=10µm
L=20µm
V_G(V)
5.d) V_D= -70V
L=2.5µm
L=5µm
L=10µm
L=20µm
$\mu_{sat.max}$(cm^2 V^{-1}s^{-1})
R_{ch}(Ω)

Figures 5(a)-(d)

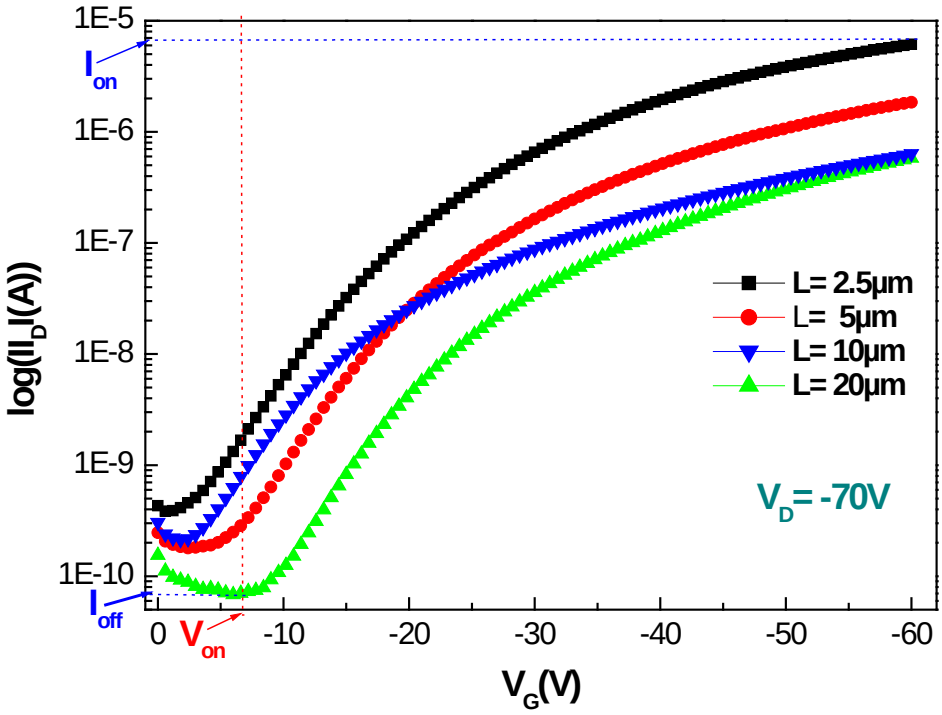
1E-5
1E-6
1E-7
1E-8
1E-9
1E-10
log(|I_D|(A))
I_on
I_off
V_on
0
-10
-20
-30
-40
-50
-60
V_G(V)
L= 2.5μm
L= 5μm
L= 10μm
L= 20μm
V_D= -70V

Figure6

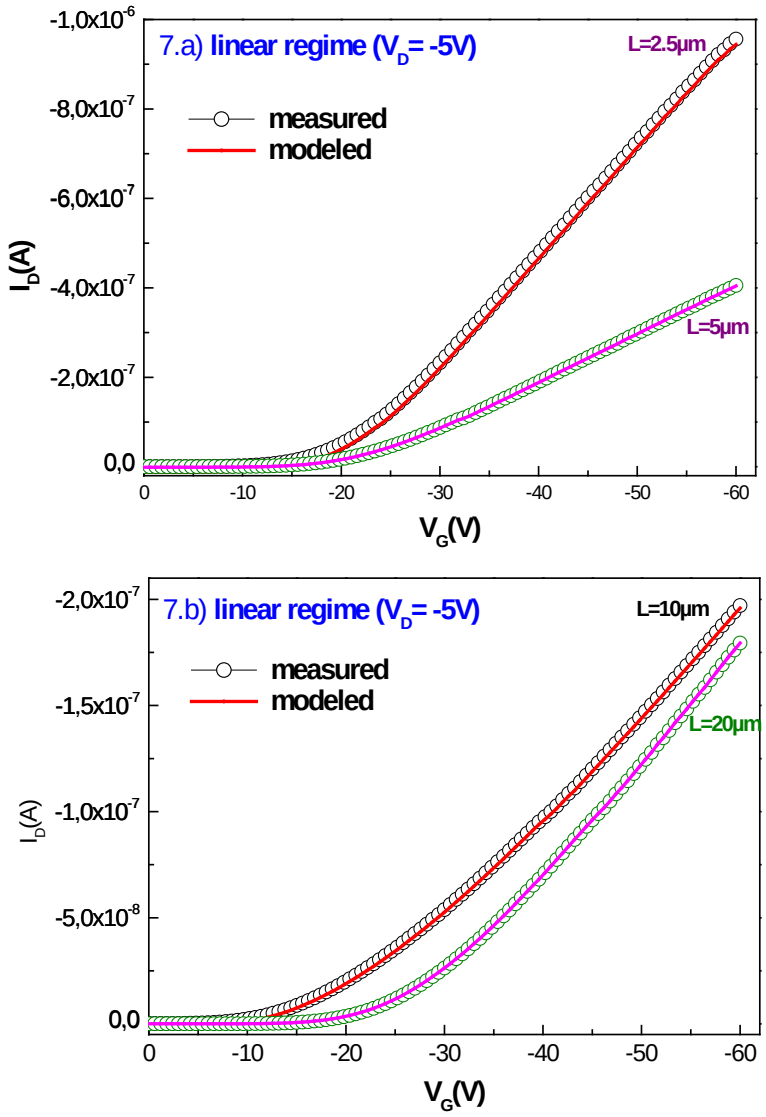
7.a) linear regime (V_D= -5V)
L=2.5µm
measured
modeled
L=5µm
I_D(A)
V_G(V)
7.b) linear regime (V_D= -5V)
L=10µm
measured
modeled
L=20µm
I_D(A)
V_G(V)

Figures 7 (a)-(b)

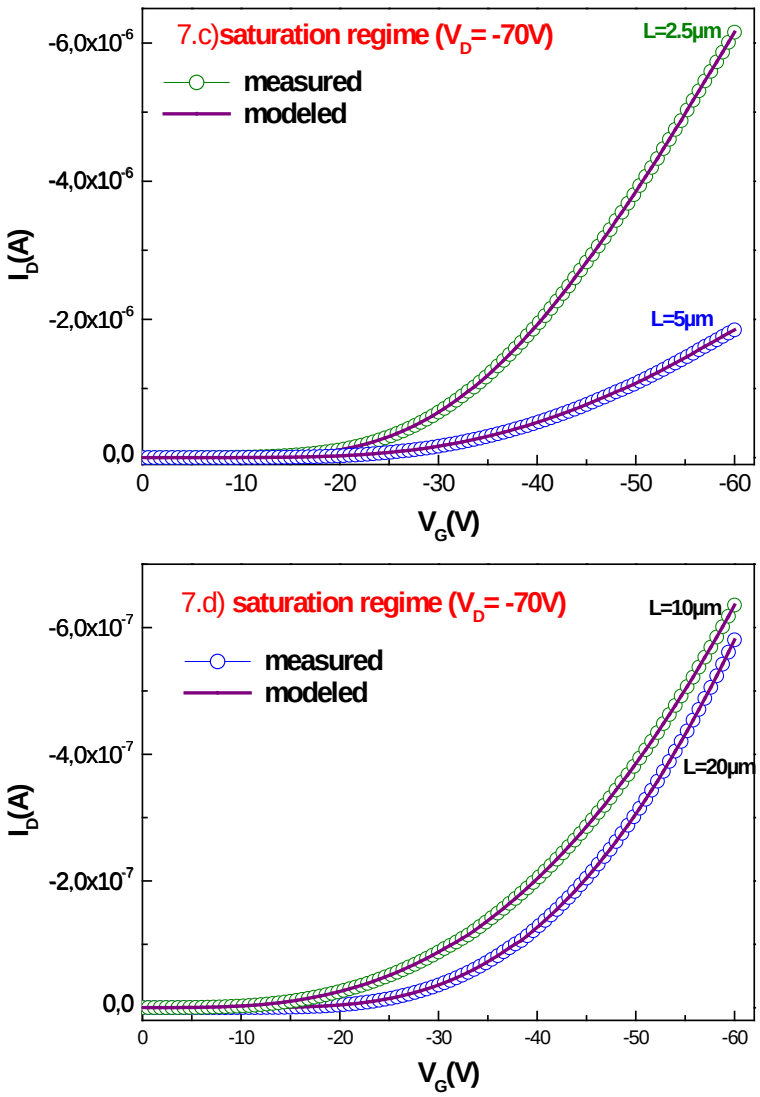
7.c)saturation regime (V_D= -70V)
measured
modeled
L=2.5µm
L=5µm
-6,0x10-6
-4,0x10-6
-2,0x10-6
0,0
I_D(A)
0
-10
-20
-30
-40
-50
-60
V_G(V)
7.d) saturation regime (V_D= -70V)
measured
modeled
L=10µm
L=20µm
-6,0x10-7
-4,0x10-7
-2,0x10-7
0,0
I_D(A)
V_G(V)

Figures 7(c)-(d)